

Testing spooky action between free-traveling electron-positron pairs

Leyun Gao,^{*} Alim Ruzi,[†] Qite Li,[‡] Chen Zhou,[§] and Qiang Li[¶]
*State Key Laboratory of Nuclear Physics and Technology,
School of Physics, Peking University, Beijing, 100871, China*

Quantum entanglement is a cornerstone of quantum mechanics. While the entanglement of confined electron pairs has been established early on, the entanglement of free-traveling electron pairs, particularly at high energies, remains largely unexplored due to the substantial challenges involved in measuring the spins of free-traveling electrons. In this study, we investigate the entanglement and the Bell inequality violation of free-traveling electron-positron pairs generated in a fixed-target experiment. This experimental setup facilitates the creation of a controllable source of entangled electron-positron pairs, where entangled events are produced in specific phase spaces. Based on this source and the prior knowledge of the entangled state, we demonstrate the feasibility of measuring the polarization correlations of the entangled e^+e^- pairs through their individual secondary scatterings off two separate additional targets.

INTRODUCTION

In quantum mechanics, many-body systems often exhibit non-classical correlations, where the state of each subsystem is interdependent with those of the others, regardless of their spatial separation. This phenomenon, known as quantum entanglement [1], is fundamental to the unique capabilities of quantum science and technology. The most distinguishing feature of quantum entanglement is the violation of Bell inequalities [2–4], which demonstrates the non-locality of our universe.

Studies of quantum entanglement in high-energy physics test quantum theory at the highest energy frontier [5–9] and provide a means to constrain free parameters in various physical models through experimental investigations [10–12]. The ATLAS Collaboration has recently observed quantum entanglement involving top quarks at a center-of-mass energy of 13 TeV, marking the highest energy measurement of quantum entanglement to date [13].

As early as 1950, Chien-Shiung Wu et al. published a paper [14] in which the angular correlation of two Compton-scattered photons arising from electron-positron annihilation are measured. This work can be considered the first experiment on quantum entanglement [15]. The experimental setup can be extended to measure correlations between free-traveling charged leptons, as will be discussed in this article.

Charged leptons in the Standard Model serve as qubits in quantum information theory, with their production, scattering, and decay processes precisely described by quantum electrodynamics. Most studies on charged lepton quantum entanglement have concentrated on the decaying tau leptons [16–22], while less attention has been given to electrons and muons. In a previous study [23], we investigated the long-neglected potential of muons for quantum state tomography and Bell inequality tests, specifically in the context of μ^-e^- scattering in muon on-target experiments, utilizing a kinematic approach [24, 25]. In this article, we examine the case

of Bhabha scattering within a similar theoretical framework. This leads to a new method for producing high-energy entangled electron-positron pairs. Both the entanglement strength and the scattering angles can benefit more from the e^+e^- final state compared to the μ^-e^- final state, as will be demonstrated numerically in the following sections.

Various experimental measurements for probing entanglement and the violation of the Bell inequality can be an eager with the entangled pair source established. Successful examples involving fixed electrons were conducted two decades ago with electron pairs confined in semiconductor quantum dots [26]. In those experiments, spin-entangled two-electron states were prepared, coherently manipulated, and measured, facilitating quantum computation within a solid-state system. However, in high energy experiments, measuring the spin of a single traveling electron poses a significant challenge due to interference from its orbital motion [27]. Instead, it is feasible to measure the average polarization of a beam of electrons or positrons by analyzing the distributions of the beam's scattering products following polarization-sensitive processes such as Mott scattering, Møller scattering, and Compton scattering [28]. Utilizing these strategies, the spin correlation of electron-positron pairs generated by positron targeting can be measured through two individual polarized secondary scattering processes: Bhabha scattering for positrons and Møller scattering for electrons. Simulation results and feasibility considerations of this proposal are presented in this article following the discussion of the entangled pair source.

THEORETICAL FRAMEWORK

After Bhabha scattering between the incoming positron and the target electron, the density matrix of the outgoing particles can be expressed as a function of kinematic quantities, specifically the scattering angles of the final state particles. Assuming that the initial state

is unpolarized, the final state density matrix ρ_f can be derived as follows:

$$\rho_{s_3' s_4' s_3 s_4} = \frac{1}{4} \sum_{s_1 s_2} \left(\frac{\mathcal{M}_{s_3' s_4' s_1 s_2} \mathcal{M}_{s_3 s_4 s_1 s_2}^*}{\sum_{s_3'' s_4''} |\mathcal{M}_{s_3'' s_4'' s_1 s_2}|^2} \right). \quad (1)$$

Here, s_1 and s_2 represent the helicities of the positron and electron before scattering, while s_3 and s_4 denote the helicities after scattering. The polarized scattering amplitude, \mathcal{M} , is calculated at the tree level as the coherent superposition of the s- and t-channel contributions.

Entanglement can be quantified by several measures [29], which are known as a class of non-negative functions called entanglement monotones [30, 31]. One such measure is *concurrence* [32–34]. For a mixed state of two qubits, the concurrence is defined as

$$\mathcal{C}(\rho_f) = \max\{0, \lambda_1 - \lambda_2 - \lambda_3 - \lambda_4\}, \quad (2)$$

where λ_i ($\lambda_i \geq \lambda_j$, $\forall i < j$) are the square roots of the eigenvalues of the matrix $\rho_f(\sigma_2 \otimes \sigma_2) \rho_f^*(\sigma_2 \otimes \sigma_2)$. If $\mathcal{C} > 0$, the two-qubit system is entangled. While $\mathcal{C}(\rho_f)$ is generally reference-frame-dependent [33], $\mathcal{C}(\rho_f)$ here inherits Lorentz invariance from the scattering amplitude \mathcal{M} .

In addition, we can test the violation of the *CHSH inequality*, $I_2 \leq 2$ [35], which is the Bell inequality for a two-qubit system, by evaluating the optimal (maximal) I_2 [36] as

$$I_2 = 2\sqrt{\lambda_1 + \lambda_2}, \quad (3)$$

where λ_1 and λ_2 are the two largest eigenvalues of the matrix $C^T C$, and C is the correlation matrix calculated by $C_{ij} = \text{Tr}(\rho_f(\sigma_i \otimes \sigma_j))$. Any value of I_2 exceeding 2 violates the CHSH form of Bell inequalities and strongly rejects the non-entanglement implications of local hidden variable theories.

ESTABLISHMENT OF A CONTROLLABLE ENTANGLED ELECTRON-POSITRON SOURCE

We use MadGraph5_aMC@NLO 3.5.5 [37] to simulate Bhabha scattering at tree-level QED, incorporating lepton masses. We consider positron beams with energies of 1, 3, and 10 GeV. Let θ_{e^-} (θ'_{e^-}) and θ_{e^+} (θ'_{e^+}) denote the polar angles of the final state electron and positron momenta in the lab (center-of-mass) frame, respectively. Within the studied energy range, spin entanglement is observed with a lower bound of approximately 1.3 rad for θ'_{μ} , in agreement with Refs. [29, 38]. Due to the symmetry illustrated in Fig. 1a and the limitations of the event generator, events with $\theta'_{e^+} > 3$ can only be generated alongside $\theta'_{e^+} < \pi - 3$, which has a significantly larger cross section, rendering the generation of the former inefficient. In this study, we focus solely on the range $\theta'_{e^+} \leq 3$ and applies the corresponding final state lepton

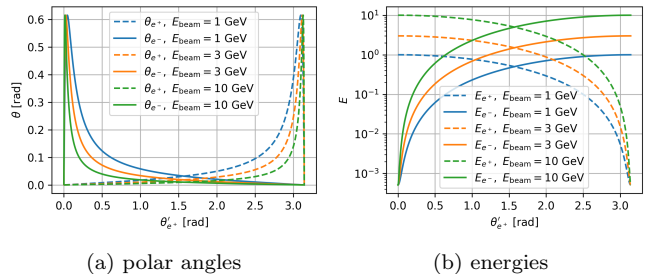


FIG. 1: (a) Polar angles θ_{e^-} and θ_{e^+} , and (b) energies E_{e^-} and E_{e^+} of the final state electron and positron in the lab frame, as functions of the polar angle of the final state positron in the center-of-mass frame, θ'_{e^+} .

pseudorapidity (η , where $\eta = -\ln[\tan(\theta/2)]$) selections in event generation.

The scatter plots in Fig. 2 illustrate the angular distributions of concurrence $\mathcal{C}(\rho_f)$ and the optimal CHSH value I_2 in both the center-of-mass and lab frames. In comparison to the results for $\mu^- e^- \rightarrow \mu^- e^-$ presented in Ref. [23], the angular ranges exhibiting entanglement witness $\mathcal{C}(\rho_f) > 0$ in the center-of-mass frame are significantly broader. The theoretical upper limits for both $\mathcal{C}(\rho_f)$ and I_2 in quantum mechanics are nearly reached as θ'_{e^+} approaches 3. For all three energies studied, over 70% of the events with $\mathcal{C}(\rho_f) > 0$ display $I_2 > 2$, thus violating the CHSH inequality. Further details are summarized in Tab. I, where $E_{e^-}^{\min}$ and $\theta_{e^+}^{\min}$ correspond to the dark blue ends of the $\mathcal{C}(\rho_f)$ plots in Fig. 2, indicating the starting points for $\mathcal{C}(\rho_f) > 0$. $E_{e^+}^{\min}$ and $\theta_{e^-}^{\min}$ correspond to the yellow ends, constrained by $\theta'_{e^+} \leq 3$.

To analyze the expected yields of entangled events in future positron on-target experiments, we define the entangled cross section σ_E as the scattering cross section σ multiplied by the ratio of events with $\mathcal{C}(\rho_f) > 0$. While entanglement can generally be measured across a broad energy range, electron-positron pairs produced under the 1 GeV configuration exhibit the most significant angular separation, making them particularly suitable for subsequent polarization correlation measurements. This configuration also yields a high production rate of entangled events. Assuming a 1 GeV positron beam with a flux of $10^{12}/\text{s}$ directed at a 10 cm thick aluminum target, the expected entangled event rate is $1.9 \times 10^9/\text{s}$. Additionally, consider the region where $0.05 \text{ rad} \leq \theta_{e^+} \leq 0.1 \text{ rad}$, which accounts for 23.4% of all events with $\mathcal{C}(\rho_f) > 0$. This region ensures $E \geq 0.094 \text{ GeV}$ and $\theta \geq 0.0103 \text{ rad}$, as shown in Fig. 1. It provides excellent measurability and electron-positron separability. It also indicates strong entanglement and a violation of the CHSH inequality, with $\mathcal{C}(\rho_f)$ reaching up to 0.953 and I_2 up to 2.8281.

By evaluating the eigenvalues and eigenvectors of the

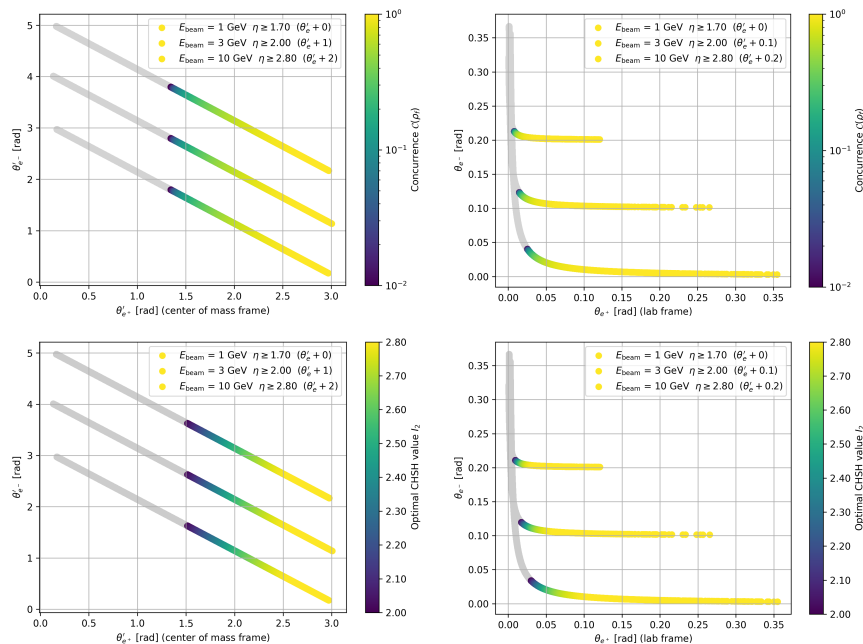


FIG. 2: Final state scatter plots colored by (top) the concurrence $\mathcal{C}(\rho_f)$ and (bottom) the optimal CHSH value I_2 . These plots correspond to various incoming positron energies in (left) the center-of-mass frame and (right) the lab frame. The light gray regions indicate where $\mathcal{C}(\rho_f) = 0$ or $I_2 \leq 2$. Events are generated with the labeled minimum pseudorapidity requirements.

TABLE I: Results on quantum entanglement and the violation of the CHSH inequality, along with the final state kinematic information, for the three studied positron beam energies.

$E_{\text{beam}}/\text{GeV}$	$E_{\text{COM}}/\text{GeV}$	$\mathcal{C}^{\text{max}}(\rho_f)$	I_2^{max}	$E_{e^+}^{\text{min}}/\text{GeV}$	$E_{e^-}^{\text{min}}/\text{GeV}$	$\theta_{e^+}^{\text{min}}/\text{rad}$	$\theta_{e^-}^{\text{min}}/\text{rad}$	$\sigma_E/\mu\text{b}$
1	0.032	0.9996	2.8281	0.008	0.389	0.0255	0.0028	243.6
3	0.055	0.9997	2.8282	0.023	1.166	0.0147	0.0016	82.1
10	0.101	0.9997	2.8282	0.074	3.890	0.0081	0.0009	26.5

arithmetic average of the density matrix ρ_f calculated in the lab frame in this region, we find that the resulting mixed state can be approximately represented as 1% $(RL + LR)/\sqrt{2}$, 1% $(RL - LR)/\sqrt{2}$, 7% $(RR - LL)/\sqrt{2}$, and 90% $(RR + LL)/\sqrt{2}$ in the lab frame. This specific state explains the near attainment of the upper limit of concurrence and the optimal CHSH value in quantum mechanics, and significantly simplifies the measurement and utilization of the resulting products. In the next section, we will focus on this region as a case study and propose an innovative approach for measuring the polarization correlation implied by this state.

MEASUREMENT OF THE FREE-TRAVELING ENTANGLED ELECTRON-POSITRON PAIRS

Measurements of electron spin trace back to the Stern-Gerlach experiment published in 1922 [39], which essentially measures the spin projection of valence electrons in silver atoms along the gradient direction of the

magnetic field. However, measuring the spin of a single traveling electron presents significant challenges. For many years following the Stern-Gerlach experiment, it was deemed impossible to spatially separate traveling electrons with different spins due to the comparable effects of the Lorentz force and the uncertainty principle on spin-induced motion [40]. It wasn't until 1997 that Stern-Gerlach-like apparatuses, similar to those proposed by Brillouin in 1928 [41], were first analytically and numerically demonstrated to achieve this separation using strong magnetic fields [40, 42–44]. Since then, various proposals have emerged to tackle this challenge, primarily focusing on minimizing the Lorentz force in novel Stern-Gerlach-like setups [45–48]. Most of these proposals target low-energy electrons and may not be effective for relativistic electrons. To date, measuring the spin of flying electrons remains a significant and fundamental research area. Despite the considerable challenges associated with measuring the spin of a single traveling electron, particularly at the GeV scale, the polarization of

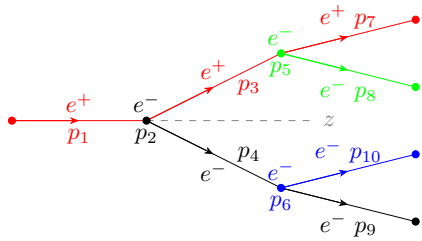


FIG. 3: Schematic diagram of the proposed cascade on-target experiment for measuring polarization correlations of the intermediate products. The circles depict the initial and final positions of the particles, while the arrows indicate their momenta. Assuming a 1 GeV incident positron beam with a flux of 10^{10} (10^{12})/s, the simultaneous production rates of four-body final states can reach the order of 1 (100)/s.

keV- to GeV-scale electron beams can be measured with a precision of 2–3% through collective scattering behaviors of beam electrons using various methods [49].

Building on the fundamental concept of measuring beam polarization correlations through polarized scattering processes, we propose a novel experimental scheme illustrated in Fig. 3. Entangled primary positron and electron beams (Particles 3 and 4) interact with electrons in two separate polarized secondary targets (Particles 5 and 6), carrying polarization information into the angular distributions of the resulting products (Particles 7–10). The electric charges of these products can be measured to distinguish the two occurred polarized processes. To minimize the number of kinematic variables involved, we measure the joint angular distribution of the two secondary scattering processes in their respective center-of-mass frames. Through this experimental setup, the previously concealed polarization correlation of the primary electron-positron pairs is transformed into the joint distribution of the two angular variables in the secondary scattering center-of-mass frames, θ'_7 and θ'_9 , which can be derived from the lab-frame angular variables measured by various detectors.

To illustrate the sensitivity of the correlation measurement, we calculate the normalized differential cross section $\frac{1}{\sigma} \frac{d^2\sigma}{d\cos\theta'_7 d\cos\theta'_9}$ using the WHIZARD Monte Carlo event generator [50, 51]. The incident positron energy is set to 1 GeV, and the primary scattering phase space is restricted to $0.05 \text{ rad} \leq \theta_3 \leq 0.1 \text{ rad}$ as elaborated in the previous section. Given the narrow angular widths of the secondary incident beams, we first consider a simplified ideal scenario where the spins of the electrons in the secondary targets (Particles 5 and 6) are always aligned with the beam direction. This setup maximizes the sensitivity to the z-component of the beam polarization. We divide the range of θ_3 into 100 bins and generate 10^5 secondary scattering events for each bin, using the midpoint

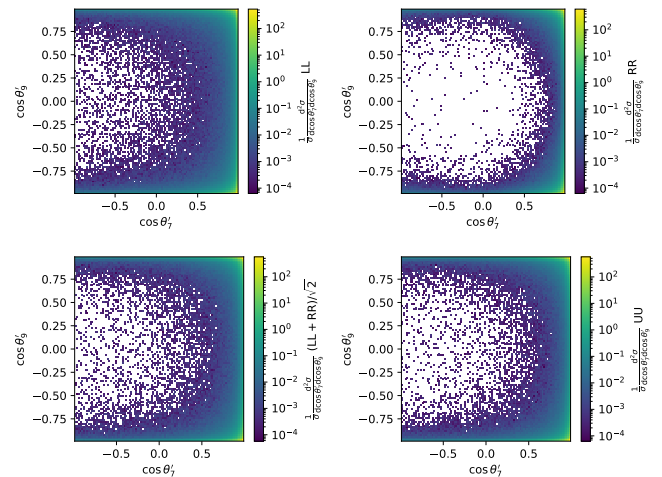


FIG. 4: Joint angular distributions of the two secondary scattering processes for four typical states of s_3s_4 . The events are simulated within the range $0.05 \text{ rad} \leq \theta_3 \leq 0.1 \text{ rad}$ for a 1 GeV positron on-target experiment and are normalized to display the density.

value of θ_3 as input. The resulting joint distributions of 4 typical polarization states of Particles 3 and 4 are presented in Fig. 4, where U denotes the unpolarized state. The events are weighted by the product of the differential cross sections of the three scattering processes and normalized to display the density. The state $(LL + RR)/\sqrt{2}$ behaves approximately as the mixed state produced by the primary scattering whose components are given in the previous section. Significant discrimination is observed among the LL , RR , and UU states, while the distinction between $(LL + RR)/\sqrt{2}$ and UU is relatively weak.

In addition to an incident positron flux of 10^{12} /s and a primary target of 10 cm thick aluminum (providing Particle 2 in Fig. 3), we also assume that the two secondary targets are 10 cm thick iron (providing Particles 5 and 6 in Fig. 3). The resulting event rate in the region where $\cos\theta'_7 \leq 0.5$ and $-0.75 \leq \theta'_9 \leq 0.75$ is 1.4×10^2 events per second for the state $(LL + RR)/\sqrt{2}$. To quantify the difference between the angular distributions resulting from the $(LL + RR)/\sqrt{2}$ and UU states, we optimize the ratio of the yields of $(LL + RR)/\sqrt{2}$ to UU in a contiguous smooth area, yielding a value of 1.29 ± 0.03 , where the uncertainty is estimated with the Poisson counting error for the Monte Carlo events. It corresponds to 4.4×10^3 post-optimization efficient signal event counts and an expected signal yield over a **27-second** run, indicating that other uncertainties, such as those from process modeling and background suppression, may dominate the real experimental analysis. The same procedure is applied to the state $(LR + RL)/\sqrt{2}$ for comparison, resulting in a ratio of 0.78 ± 0.02 .

For the 20% polarized targets, the ratios are 1.010 ± 0.009 and 0.986 ± 0.009 generated from 25 times the num-

ber of Monte Carlo events of the 100% polarized targets to reduce counting errors, with resolving power still present. For the $(LL + RR)/\sqrt{2}$ signal, it corresponds to 2.5×10^4 efficient event counts accumulated in **680 seconds**. The high event rate holds, indicating a promising potential to mitigate the decline in resolving power associated with low target polarization purities in real-world applications.

Despite the representability of the θ'_7 - θ'_9 correlation to the s_3 - s_4 correlation and the promising potential event rates for the cascade scattering experiment, reconstructing the density matrix $\rho_{s'_3 s'_4 s_3 s_4}$ from the secondary scattering products presents a significant challenge. A 4×4 density matrix is typically defined by 15 independent real parameters, which is considerably more than the four pure states we have examined. For arbitrary mixed states, we find significant degeneracy among them which complicates the quantitative reconstruction of the density matrix. However, the correlation effects can still be investigated, and a simplified state tomography can be performed assuming prior knowledge from the primary scattering, which indicates that approximately only a few linear combinations of the bases RR , RL , LR , and LL exist. We encourage the community to further explore the potential of this innovative approach. We believe that establishing a viable method for performing direct quantum state tomography on high-energy scattering products would represent a significant advancement in the field of quantum science.

SUMMARY AND OUTLOOK

In a GeV-order positron on-target experiment, highly entangled electron-positron pairs can be efficiently produced through Bhabha scattering. By filtering events based on specific scattering angles, it is possible to select events with particular levels of entanglement and energies for each entangled particle. This method enables the creation of a controllable source of entangled electron-positron pairs. Simulations with incident positron energies of 1, 3, and 10 GeV yield concurrence values close to one, along with optimal CHSH values near $2\sqrt{2}$ under extreme conditions. These indicators remain promising across a wide range of the lab frame phase space suitable for electron-positron separation and measurements. Although measuring the spin state of a free-traveling electron or positron presents a significant challenge, it is feasible to measure the average polarizations of electron and positron beams. We found that these strategies are generalizable for measuring the polarization correlations of the electron-positron pairs produced by positron targeting through secondary polarized scatterings. Similar studies can also be conducted in electron on-target experiments.

ACKNOWLEDGMENTS

This work is supported in part by the National Natural Science Foundation of China under Grants No. 12325504, and No. 12061141002.

* seeson@pku.edu.cn

† alim.ruzi@pku.edu.cn

‡ liqt@pku.edu.cn

§ czhouphy@pku.edu.cn

¶ qliphy0@pku.edu.cn

- [1] A. Einstein, B. Podolsky, and N. Rosen, Can quantum mechanical description of physical reality be considered complete?, *Phys. Rev.* **47**, 777 (1935).
- [2] J. S. Bell, On the Einstein-Podolsky-Rosen paradox, *Physics Physique Fizika* **1**, 195 (1964).
- [3] S. J. Freedman and J. F. Clauser, Experimental Test of Local Hidden-Variable Theories, *Phys. Rev. Lett.* **28**, 938 (1972).
- [4] J. F. Clauser and A. Shimony, Bell's theorem: Experimental tests and implications, *Rept. Prog. Phys.* **41**, 1881 (1978).
- [5] M. Fabbrichesi, R. Floreanini, and G. Panizzo, Testing Bell Inequalities at the LHC with Top-Quark Pairs, *Phys. Rev. Lett.* **127**, 161801 (2021), arXiv:2102.11883 [hep-ph].
- [6] A. J. Barr, Testing Bell inequalities in Higgs boson decays, *Phys. Lett. B* **825**, 136866 (2022), arXiv:2106.01377 [hep-ph].
- [7] R. Ashby-Pickering, A. J. Barr, and A. Wierzychucka, Quantum state tomography, entanglement detection and Bell violation prospects in weak decays of massive particles, *JHEP* **05**, 020, arXiv:2209.13990 [quant-ph].
- [8] M. Fabbrichesi, R. Floreanini, E. Gabrielli, and L. Marzola, Bell inequalities and quantum entanglement in weak gauge boson production at the LHC and future colliders, *Eur. Phys. J. C* **83**, 823 (2023), arXiv:2302.00683 [hep-ph].
- [9] A. J. Barr, M. Fabbrichesi, R. Floreanini, E. Gabrielli, and L. Marzola, Quantum entanglement and Bell inequality violation at colliders, *Prog. Part. Nucl. Phys.* **139**, 104134 (2024), arXiv:2402.07972 [hep-ph].
- [10] M. Fabbrichesi, R. Floreanini, and E. Gabrielli, Constraining new physics in entangled two-qubit systems: top-quark, tau-lepton and photon pairs, *Eur. Phys. J. C* **83**, 162 (2023), arXiv:2208.11723 [hep-ph].
- [11] M. Fabbrichesi and L. Marzola, Dipole momenta and compositeness of the τ lepton at Belle II, *Phys. Rev. D* **109**, 095026 (2024), arXiv:2401.04449 [hep-ph].
- [12] P. Lo Chiatto, Interference Resurrection of the τ Dipole through Quantum Tomography (2024) arXiv:2408.04553 [hep-ph].
- [13] G. Aad *et al.* (ATLAS), Observation of quantum entanglement with top quarks at the ATLAS detector, *Nature* **633**, 542 (2024), arXiv:2311.07288 [hep-ex].
- [14] C. S. Wu and I. Shaknov, The Angular Correlation of Scattered Annihilation Radiation, *Phys. Rev.* **77**, 136 (1950).

- [15] C. N. Yang, C. S. Wu's Contributions: A Retrospective in 2015, *Int. J. Mod. Phys. A* **30**, 1530050 (2015).
- [16] J. Babson and E. Ma, Decay Product Correlation of $\tau^+\tau^-$ From e^+e^- Annihilation, *Phys. Rev. D* **26**, 2497 (1982).
- [17] P. Privitera, Decay correlations in $e^+e^- \rightarrow \tau^+\tau^-$ as a test of quantum mechanics, *Phys. Lett. B* **275**, 172 (1992).
- [18] H. K. Dreiner, Bell's inequality and tau physics at LEP, in *2nd Workshop on Tau Lepton Physics* (1992) arXiv:hep-ph/9211203.
- [19] K. Ehatäht, M. Fabbrichesi, L. Marzola, and C. Veelken, Probing entanglement and testing Bell inequality violation with $e^+e^- \rightarrow \tau^+\tau^-$ at Belle II, *Phys. Rev. D* **109**, 032005 (2024), arXiv:2311.17555 [hep-ph].
- [20] K. Ma and T. Li, Testing Bell inequality through $H \rightarrow \tau\tau$ at CEPC, *Chin. Phys. C* **48**, 103105 (2024), arXiv:2309.08103 [hep-ph].
- [21] M. M. Altakach, P. Lamba, F. Maltoni, K. Mawatari, and K. Sakurai, Quantum information and CP measurement in $H \rightarrow \tau^+\tau^-$ at future lepton colliders, *Phys. Rev. D* **107**, 093002 (2023), arXiv:2211.10513 [hep-ph].
- [22] M. Fabbrichesi and L. Marzola, Quantum tomography with τ leptons at the FCC-ee: Entanglement, Bell inequality violation, $\sin\theta_W$, and anomalous couplings, *Phys. Rev. D* **110**, 076004 (2024), arXiv:2405.09201 [hep-ph].
- [23] L. Gao, A. Ruzi, Q. Li, C. Zhou, L. Chen, X. Zhang, Z. Sun, and Q. Li, Quantum state tomography with muons (2024) arXiv:2411.12518 [hep-ph].
- [24] S. Fedida and A. Serafini, Tree-level entanglement in quantum electrodynamics, *Phys. Rev. D* **107**, 116007 (2023).
- [25] K. Cheng, T. Han, and M. Low, Quantum Tomography at Colliders: With or Without Decays (2024) arXiv:2410.08303 [hep-ph].
- [26] J. R. Petta, A. C. Johnson, J. M. Taylor, E. A. Laird, A. Yacoby, M. D. Lukin, C. M. Marcus, M. P. Hanson, and A. C. Gossard, Coherent Manipulation of Coupled Electron Spins in Semiconductor Quantum Dots, *Science* **309**, 1116955 (2005).
- [27] B. M. Garraway and S. Stenholm, Does a flying electron spin?, *Contemporary Physics* **43**, 147 (2002).
- [28] D. Gaskell, Electron polarimetry, in *Polarized Beam Dynamics and Instrumentation in Particle Accelerators: USPAS Summer 2021 Spin Class Lectures*, edited by F. Méot, H. Huang, V. Ptitsyn, and F. Lin (Springer International Publishing, Cham, 2023) pp. 301–314.
- [29] S. Fedida and A. Serafini, Tree-level entanglement in quantum electrodynamics, *Phys. Rev. D* **107**, 116007 (2023), arXiv:2209.01405 [quant-ph].
- [30] R. Horodecki, P. Horodecki, M. Horodecki, and K. Horodecki, Quantum entanglement, *Rev. Mod. Phys.* **81**, 865 (2009), arXiv:quant-ph/0702225.
- [31] E. Chitambar and G. Gour, Quantum resource theories, *Rev. Mod. Phys.* **91**, 025001 (2019), arXiv:1806.06107 [quant-ph].
- [32] W. K. Wootters, Entanglement of formation of an arbitrary state of two qubits, *Phys. Rev. Lett.* **80**, 2245 (1998), arXiv:quant-ph/9709029.
- [33] R. M. Gingrich and C. Adami, Quantum Entanglement of Moving Bodies, *Phys. Rev. Lett.* **89**, 270402 (2002), arXiv:quant-ph/0205179.
- [34] S. Hill and W. K. Wootters, Entanglement of a pair of quantum bits, *Phys. Rev. Lett.* **78**, 5022 (1997), arXiv:quant-ph/9703041.
- [35] J. F. Clauser, M. A. Horne, A. Shimony, and R. A. Holt, Proposed experiment to test local hidden variable theories, *Phys. Rev. Lett.* **23**, 880 (1969).
- [36] R. Horodecki, P. Horodecki, and M. Horodecki, Violating Bell inequality by mixed spin-1/2 states: necessary and sufficient condition, *Phys. Lett. A* **200**, 340 (1995).
- [37] J. Alwall, R. Frederix, S. Frixione, V. Hirschi, F. Maltoni, O. Mattelaer, H. S. Shao, T. Stelzer, P. Torrielli, and M. Zaro, The automated computation of tree-level and next-to-leading order differential cross sections, and their matching to parton shower simulations, *JHEP* **07**, 079, arXiv:1405.0301 [hep-ph].
- [38] A. Cervera-Lierta, J. I. Latorre, J. Rojo, and L. Rottoli, Maximal Entanglement in High Energy Physics, *SciPost Phys.* **3**, 036 (2017), arXiv:1703.02989 [hep-th].
- [39] W. Gerlach and O. Stern, Experimental test of the applicability of the quantum theory to the magnetic field, *Z. Phys.* **9**, 349 (1922).
- [40] H. Batelaan, T. J. Gay, and J. J. Schwendiman, Stern-Gerlach effect for electron beams, *Phys. Rev. Lett.* **79**, 4517 (1997).
- [41] L. Brillouin, Is it possible to test by a direct experiment the hypothesis of the spinning electron?, *Proceedings of the National Academy of Sciences* **14**, 755 (1928).
- [42] G. H. Rutherford and R. Grobe, Comment on "stern-gerlach effect for electron beams", *Phys. Rev. Lett.* **81**, 4772 (1998).
- [43] H. Batelaan and T. J. Gay, Batelaan and gay reply:, *Phys. Rev. Lett.* **81**, 4773 (1998).
- [44] B. M. Garraway and S. Stenholm, Observing the spin of a free electron, *Phys. Rev. A* **60**, 63 (1999).
- [45] S. McGregor, R. Bach, and H. Batelaan, Transverse quantum stern-gerlach magnets for electrons, *New Journal of Physics* **13**, 065018 (2011).
- [46] M. Kohda, S. Nakamura, Y. Nishihara, K. Kobayashi, T. Ono, J.-i. Ohe, Y. Tokura, T. Mineno, and J. Nitta, Spin-orbit induced electronic spin separation in semiconductor nanostructures, *Nature communications* **3**, 1082 (2012).
- [47] M. M. Dellweg and C. Müller, Spin-Polarizing Interferometric Beam Splitter for Free Electrons, *Phys. Rev. Lett.* **118**, 070403 (2017), arXiv:1607.08793 [quant-ph].
- [48] A. Ghazaryan, M. Lemeshko, and A. G. Volosniev, Filtering spins by scattering from a lattice of point magnets, *Communications Physics* **3**, 178 (2020), arXiv:2004.04511 [cond-mat.mes-hall].
- [49] K. Aulenbacher, E. Chudakov, D. Gaskell, J. Grames, and K. D. Paschke, Precision electron beam polarimetry for next generation nuclear physics experiments, *Int. J. Mod. Phys. E* **27**, 1830004 (2018).
- [50] W. Kilian, T. Ohl, and J. Reuter, WHIZARD: Simulating Multi-Particle Processes at LHC and ILC, *Eur. Phys. J. C* **71**, 1742 (2011), arXiv:0708.4233 [hep-ph].
- [51] M. Moretti, T. Ohl, and J. Reuter, O'Mega: An Optimizing matrix element generator (2001), arXiv:hep-ph/0102195.